Chapter 4

Jet pinch-off in liquid-liquid systems with surface tension

4.1 Introduction

Breakup of a liquid column surrounded by another fluid has been of great interest for many years and investigations date to Savart (1833), Rayleigh (1878), and Weber (1931). The breakup problem is considered to be one of the classical problems of fluid mechanics and is a fundamental feature of many engineering, industrial and biomedical applications.

Liquid-liquid and liquid-gas jets can be found in many industrial applications including ink-jet printers, internal combustion engines, chemical reactors, oil-water separators and fuel atomizers. In liquid-liquid extractors used in chemical processing, emulsions of small droplets are generated in order to increase interfacial area and hence mass transfer. The size distribution of the droplets thus has a direct effect on mass transfer rates. In ink-jet printers, droplets of uniform size are desired. A problem arises when small satellite drops form between the larger primary droplets during the pinch-off process. In both of these examples, it can be seen that the dynamics of pinch-off, including whether or not satellites form, directly affects system performance. In order to optimize and control performance, then, it is necessary to understand the mechanism governing pinch-off [98].

In the case of liquid/gas interfaces and liquid/liquid interfaces in Stokes flows, possible to develop physically-based reconnection conditions by using a lubrication theory to derive special similarity solutions of the equations (see [86, 59, 60, 133]). However, when there is significant competition between inertia, viscosity and surface tension, the dynamics of topology transitions are much more complicated

than in the fluid-gas case and no such similarity solutions are known.

In these flows, the surface tension may cause the jet to become unstable to axisymmetric perturbations, eventually leading to its break-up. This breakup can cause overturning in the interface rendering lubrication approximations invalid. See Fig. 4.4 for example. This instability is referred to the Rayleigh instability after Rayleigh who studied the break-up of water jets in air [108]. The Rayleigh instability is responsible for much of the break-up of liquid drops observed in real fluid flows.

To capture the break-up, we will use the NSCH system where the (**C-H**) equation is implemented with degenerate mobility. We first develop numerical methods for the axisymmetric Cahn-Hilliard equation and the axisymmetric Navier-Stokes equation in the cylindrical coordinates separately and couple them to obtain a numerical method for the axisymmetric NSCH equations. We will focus on Boussinesq approximation in which density varies only in the gravity term.

In this chapter, we will also present comparisons of numerical method with an experiment performed by Ilija Milosevic in Professor Ellen Longmire's laboratory (Dept. Aerospace and Mechanics, U. Minn.) [98].

4.2 Governing Equations

Let $\rho_1,\ \rho_2$ and $\mathbf{u}_1,\ \mathbf{u}_2$ be the densities (m_i/V) and velocities of the two fluid components, respectively. Let $\rho = \rho(c)$ be the total density m/V and $\mathbf{u}$ be the mass-averaged velocity field, i.e., $\rho\mathbf{u} = \rho_1\mathbf{u}_1 + \rho_2\mathbf{u}_2$. Then, in dimensional form, the NSCH equations [89] are

$$\nabla \cdot \mathbf{u} = -\frac{\rho'(c)}{\rho}\dot{c}, \tag{4.2.1}$$

$$\rho\dot{\mathbf{u}} = -\nabla p + \nabla \cdot (\eta(\nabla\mathbf{u} + \nabla\mathbf{u}^T)) + \nabla(\lambda\nabla\cdot\mathbf{u}) - \sigma\epsilon\nabla\cdot(\rho\nabla c\otimes\nabla c) + \rho g\mathbf{G} \tag{4.2.2}$$

$$\rho\dot{c} = \nabla\cdot(M(c)\nabla\mu), \tag{4.2.3}$$

where $\cdot = \partial_t + \mathbf{u}\cdot\nabla$ is the advective derivative, $\rho = \rho(c)$ is the density, $\mathbf{u} = (u, w)$ is the velocity, p is the pressure, λ and η are the viscosity coefficients, $\mathbf{G} = (0, -1)$, and $'$ denotes the derivative with respect to c. μ is the generalized chemical potential given by

$$\mu = f(c) - \frac{\rho'(c)}{\rho^2}[p - (\lambda + 2\eta/3)\nabla\cdot\mathbf{u}] - \frac{\epsilon^2}{\rho}\nabla\cdot(\rho\nabla c), \tag{4.2.4}$$

where $f(c)$ is the Helmholtz free energy.

We will consider a simple mixture of two fluids in which density is defined by

$$\frac{1}{\rho} = \frac{c}{\rho_1} + \frac{1-c}{\rho_2}$$

so that if $\alpha = 1/\rho_1 - 1/\rho_2$, then

$$\rho(c) = \frac{1}{\alpha c + \frac{1}{\rho_2}}. \tag{4.2.5}$$

Then from (4.2.5) it follows that

$$\frac{\rho'}{\rho^2} = -\alpha,$$

therefore the equation (4.2.1) becomes $\nabla \cdot \mathbf{u} = \alpha\rho\dot{c}$.

A broad range of variable density flows have small density variations that can be modeled using a Boussinesq approximation. (See Chandrasekhar [34] for a detailed discussion of the Boussinesq approximation.) In the Boussinesq approximation density variations are assumed to be sufficiently small but $\Delta\rho g \sim O(1)$ so that the density is constant (ρ_*) except in the gravitational term. Also we define

$$q = p + \rho\sigma\epsilon|\nabla c|^2,$$

and using the vector identity

$$\nabla \cdot (\rho\nabla c \otimes \nabla c) = \nabla(\rho|\nabla c|^2) + \rho(\Delta c\nabla c - \frac{1}{2}\nabla|\nabla c|^2),$$

then the NSCH equations (4.2.1-4.2.4) with the Boussinesq limit can be written as

$$\begin{aligned}
\nabla \cdot \mathbf{u} &= 0, && (4.2.6)\\
\rho_*\dot{\mathbf{u}} &= -\nabla q + \nabla \cdot (\eta(\nabla\mathbf{u} + \nabla\mathbf{u}^T)) - \rho_*\sigma\epsilon(\Delta c\nabla c - \frac{1}{2}\nabla|\nabla c|^2) + \rho g\mathbf{G} && (4.2.7)\\
\rho_*\dot{c} &= \nabla \cdot (M(c)\nabla\mu), && (4.2.8)\\
\mu &= f(c) - \epsilon^2\Delta c, && (4.2.9)
\end{aligned}$$

The next step is to restate the dimensional NSCH equations in dimensionless form and for this purpose we define characteristic values such as length, velocity, time, etc. We can then introduce dimensionless ratios for the space coordinates, time, the velocity components, and the fluid pressure.

$$\bar{x} = \frac{x}{L_*}, \quad \bar{t} = \frac{V_* t}{L_*}, \quad \bar{\mathbf{u}} = \frac{\mathbf{u}}{V_*}, \quad \bar{\epsilon} = \frac{\epsilon}{L_*}, \quad \bar{q} = \frac{q}{\rho_* V_*^2}, \quad \bar{\eta} = \frac{\eta}{\eta_*}, \quad \bar{\mu}_* = \frac{\rho_*\mu}{p_*}, \quad \bar{\rho} = \frac{\rho}{\Delta\rho}, \tag{4.2.10}$$

If we now substitute in (4.2.7) from (4.2.10) we get:

$$\begin{aligned}
\rho_*(\frac{V_*^2}{L_*}\bar{\mathbf{u}}_{\bar{t}} + \frac{V_*^2}{L_*}\bar{\mathbf{u}} \cdot \nabla\bar{\mathbf{u}}) &= -\frac{\rho_* V_*^2}{L_*}\nabla\bar{q} + \frac{\eta_* V_*}{L_*^2}\nabla \cdot [\bar{\eta}(\nabla\bar{\mathbf{u}} + \nabla\bar{\mathbf{u}}^T)] \qquad (4.2.11)\\
&\quad -\frac{\rho_*\sigma\bar{\epsilon}}{L_*^2}(\Delta c\nabla c - \frac{1}{2}\nabla|\nabla c|^2) + \rho_*\bar{\rho}g\mathbf{G}.
\end{aligned}$$

After dividing by $\frac{\rho_* V_*^2}{L_*}$ in equation (4.2.11), we get:

$$\begin{aligned}
\bar{\mathbf{u}}_{\bar{t}} + \bar{\mathbf{u}} \cdot \nabla\bar{\mathbf{u}} &= -\nabla\bar{q} + \frac{\eta_*}{\rho_* L_* V_*}\nabla \cdot [\bar{\eta}(\nabla\bar{\mathbf{u}} + \nabla\bar{\mathbf{U}}^T)]\\
&\quad -\frac{\rho_*\sigma\bar{\epsilon}}{\rho_* L_* V_*^2}(\Delta c\nabla c - \frac{1}{2}\nabla|\nabla c|^2) + \frac{\Delta\rho g L_*}{\rho_* V_*^2}\frac{\rho_*}{\Delta\rho}\bar{\rho}\mathbf{G}.
\end{aligned}$$

If we now substitute in (4.2.8) from (4.2.10) we get:

$$\rho_*(\frac{V_*}{L_*}\bar{c}_{\bar{t}} + \frac{V_*}{L_*}\bar{\mathbf{u}}\cdot\nabla\bar{c}) = \frac{\mu_* M_*}{L_*^2}\nabla\cdot(\bar{M}(c)\nabla\bar{\mu}), \tag{4.2.12}$$

After dividing by $\frac{\rho_* V_*}{L_*}$ in equation (4.2.12), we get:

$$c_{\bar{t}} + \bar{\mathbf{u}}\cdot\nabla c = \frac{\mu_* M_*}{\rho_* L_*^2 V_*}\nabla\cdot(\bar{M}(c)\nabla\bar{\mu}), \tag{4.2.13}$$

Letting $\epsilon = \rho_*\bar{\epsilon},\ \rho = \rho_*\bar{\rho}/\Delta\rho$, dropping the bar notations and using the dimensionless numbers, the dimensionless equations reduce to

$$\begin{aligned}
\mathbf{u}_t + \mathbf{u}\cdot\nabla\mathbf{u} &= -\nabla q + \frac{1}{\mathbf{Re}}\nabla\cdot[\eta(c)(\nabla\mathbf{u} + \nabla\mathbf{u}^T)] \qquad (4.2.14)\\
&\quad -\frac{\epsilon}{\mathbf{We}}(\Delta c\nabla c - \frac{1}{2}\nabla|\nabla c|^2) + \frac{\rho(c)}{\mathbf{Fr}^2}\mathbf{G},\\
\nabla\cdot\mathbf{u} &= 0, \qquad (4.2.15)\\
c_t + \mathbf{u}\cdot\nabla c &= \frac{1}{\mathbf{Pe}}\nabla\cdot(M(c)\nabla\mu), \qquad (4.2.16)\\
\mu &= f(c) - \mathbf{C}\Delta c. \qquad (4.2.17)
\end{aligned}$$

where the Reynolds number is

$$\mathbf{Re} = \rho_* V_* L_*/\eta_*,$$

the Froude number is

$$\mathbf{Fr} = V_*\sqrt{\rho_*}/\sqrt{\Delta\rho g L_*},$$

the Weber number is

$$\mathbf{We} = \rho_* L_* V_*^2/\sigma,$$

the Cahn number is

$$\mathbf{C} = \epsilon^2/\mu_*,$$

and the diffusional Peclet number is

$$\mathbf{Pe} = \rho_* L_* V_*/(M_*\mu_*).$$

In the above dimensionless groups, the characteristic scales depend on the application. For example, L_* is typically taken to be a characteristic diameter of a thread or jet, V_* is typically taken to be the surface tension velocity $\sim \sigma/\eta_0$. In the case of the jet, V_* is taken to be the jet exit velocity.

Next, let the forcing term in the Navier-Stokes equation be

$$\mathbf{F} = (F_1, F_2, F_3) = -\frac{\epsilon}{\mathbf{We}}(\Delta c\nabla c - \frac{1}{2}\nabla|\nabla c|^2) + \frac{\rho(c)}{\mathbf{Fr}^2}\mathbf{G}.$$

where

$$\Delta = \frac{1}{r}\partial_r + \partial_r^2 + \partial_z^2, \qquad \nabla = (\partial_r, \partial_z), \qquad \nabla\cdot(u, w) = \frac{1}{r}\frac{\partial(ru)}{\partial r} + \frac{\partial w}{\partial z}.$$

2.A Projection Method

We use the version of the projection method based on the pressure increment formulation developed by Bell *et al* [15].

$$\begin{aligned}\frac{\mathbf{u}^* - \mathbf{u}^n}{\Delta t} + \nabla p^{n-\frac{1}{2}} &= \frac{1}{2\mathbf{Re}}\nabla\cdot\eta(c^{n+1})[\nabla\mathbf{u}^* + (\nabla\mathbf{u}^*)^T] \\ &\quad + \frac{1}{2\mathbf{Re}}\nabla\cdot\eta(c^n)[\nabla\mathbf{u}^n + (\nabla\mathbf{u}^n)^T] - (\mathbf{u}\cdot\nabla\mathbf{u})^{n+\frac{1}{2}} + \mathbf{F}^{n+\frac{1}{2}}, \\ \nabla\cdot\mathbf{u}^{n+1} &= 0.\end{aligned} \tag{4.2.18}$$

For $\mathbf{u}$ defined at cell centers and p defined at cell corners, discrete differential operators are defined as follows:

$$(\nabla p)_{ij} = \begin{pmatrix} \frac{p_{i+\frac{1}{2},j+\frac{1}{2}} + p_{i+\frac{1}{2},j-\frac{1}{2}} - p_{i-\frac{1}{2},j+\frac{1}{2}} - p_{i-\frac{1}{2},j-\frac{1}{2}}}{2\Delta r} \\ \\ \frac{p_{i+\frac{1}{2},j+\frac{1}{2}} + p_{i-\frac{1}{2},j+\frac{1}{2}} - p_{i+\frac{1}{2},j-\frac{1}{2}} - p_{i-\frac{1}{2},j-\frac{1}{2}}}{2\Delta z} \end{pmatrix}$$

$$(\nabla\cdot(u,w))_{ij} = \frac{r_{i+1}u_{i+1,j} - r_{i-1}u_{i-1,j}}{2r_i\Delta r} + \frac{w_{i,j+1} - w_{i,j-1}}{2\Delta z}$$

$$(\Delta u)_{ij} = \frac{r_{i+\frac{1}{2}}(u_{i+1,j} - u_{ij}) - r_{i-\frac{1}{2}}(u_{ij} - u_{i-1,j})}{r_i\Delta r^2} + \frac{u_{i,j+1} - 2u_{ij} + u_{i,j-1}}{\Delta z^2}$$

$$\begin{aligned}\nabla\cdot[\eta(\nabla\mathbf{u} + \nabla\mathbf{u}^T)] &= \nabla\cdot\left[\eta\begin{pmatrix} 2u_r & 0 & u_z + w_r \\ 0 & \frac{1}{r}u & 0 \\ u_z + w_r & 0 & 2w_z \end{pmatrix}\right] \\ &= \begin{bmatrix} \frac{2}{r}(r\eta u_r)_r - \frac{\eta}{r^2}u + (\eta u_z)_z + (\eta w_r)_z \\ \frac{1}{r}(r\eta u_z)_r + \frac{1}{r}(r\eta w_r)_r + 2(\eta w_z)_z \end{bmatrix}.\end{aligned}$$

$$(\mathcal{L})^1_{ij} = \begin{pmatrix} \frac{2r_{i+\frac{1}{2}}\eta_{i+\frac{1}{2},j}(u_{i+1,j} - u_{ij}) - 2r_{i-\frac{1}{2}}\eta_{i-\frac{1}{2},j}(u_{ij} - u_{i-1,j})}{r_i\Delta r^2} \\ \\ -\frac{\eta_{ij}}{r_i^2}u_{ij} + \frac{\eta_{i,j+\frac{1}{2}}(u_{i,j+1} - u_{ij}) - \eta_{i,j-\frac{1}{2}}(u_{ij} - u_{i,j-1})}{\Delta z^2} \\ \\ + \frac{\eta_{i,j+\frac{1}{2}}(w_{i+1,j+1} - w_{i-1,j+1} + w_{i+1,j} - w_{i-1,j})}{4\Delta r\Delta z} \\ \\ - \frac{\eta_{i,j-\frac{1}{2}}(w_{i+1,j} - w_{i-1,j} + w_{i+1,j-1} - w_{i-1,j-1})}{4\Delta r\Delta z} \end{pmatrix},$$

$$(\mathcal{L})^2_{ij} = \begin{pmatrix} \frac{r_{i+\frac{1}{2}}\eta_{i+\frac{1}{2},j}(u_{i+1,j+1}-u_{i+1,j-1}+u_{i,j+1}-u_{i,j-1})}{4r_i\Delta r\Delta z} \\ -\frac{r_{i-\frac{1}{2}}\eta_{i-\frac{1}{2},j}(u_{i,j+1}-u_{i,j-1}+u_{i-1,j+1}-u_{i-1,j-1})}{4r_i\Delta r\Delta z} \\ +\frac{r_{i+\frac{1}{2}}\eta_{i+\frac{1}{2},j}(w_{i+1,j}-w_{ij})-r_{i-\frac{1}{2}}\eta_{i-\frac{1}{2},j}(w_{ij}-w_{i-1,j})}{r_i\Delta r^2} \\ +\frac{2\eta_{i,j+\frac{1}{2}}(w_{i,j+1}-w_{ij})-2\eta_{i,j-\frac{1}{2}}(w_{ij}-w_{i,j-1})}{\Delta z^2} \end{pmatrix},$$

where

$$\begin{aligned} r_{i+\frac{1}{2}} &= \frac{1}{2}(r_{i+1,j}+r_i), \\ \eta_{i+\frac{1}{2},j} &= \frac{1}{2}[\eta(c_{ij})+\eta(c_{i+1,j})], \\ \eta_{i,j+\frac{1}{2}} &= \frac{1}{2}[\eta(c_{ij})+\eta(c_{i,j+1})]. \end{aligned}$$

Let's rewrite Eq. (4.2.18)

$$\begin{aligned} \mathbf{u}^* - \frac{\Delta t}{2\mathbf{Re}}\nabla\cdot[\eta^{n+1}(\nabla\mathbf{u}^* + (\nabla\mathbf{u}^*)^T)] &= \mathbf{u}^n - \Delta t[\mathbf{u}\cdot\nabla\mathbf{u}]^{n+\frac{1}{2}} - \Delta t\nabla p^{n-\frac{1}{2}} \\ &+ \frac{\Delta t}{2\mathbf{Re}}\nabla\cdot[\eta^n(\nabla\mathbf{u}^n + (\nabla\mathbf{u}^*)^T)] + \Delta t\mathbf{F}^{n+\frac{1}{2}} \end{aligned} \tag{4.2.19}$$

Let right hand side of equation (4.2.19) be S^n.

Then we have

$$\mathbf{u}^* - \frac{\Delta t}{2\mathbf{Re}}\nabla\cdot[\eta^{n+1}(\nabla\mathbf{u}^* + (\nabla\mathbf{u}^*)^T)] = S^n = ({s_1}^n, {s_2}^n),$$

$$\begin{aligned} &[1+\frac{\Delta t}{2h^2\mathbf{Re}}(\frac{2r_{i+\frac{1}{2}}\eta_{i+\frac{1}{2},j}+2r_{i-\frac{1}{2}}\eta_{i-\frac{1}{2},j}}{r_i}+\frac{\eta_{ij}h^2}{r_i^2}+\eta_{i,j+\frac{1}{2}}+\eta_{i,j-\frac{1}{2}})]u^*_{i,j} = {s_1}^n \\ &+\frac{\Delta t}{2h^2\mathbf{Re}}[\frac{2r_{i+\frac{1}{2}}\eta_{i+\frac{1}{2},j}u_{i+1,j}+2r_{i-\frac{1}{2}}\eta_{i-\frac{1}{2},j}u_{i-1,j}}{r_i}+\eta_{i,j+\frac{1}{2}}u_{i,j+1}+\eta_{i,j-\frac{1}{2}}u_{i,j-1} \\ &+\frac{\eta_{i,j+\frac{1}{2}}(w_{i+1,j+1}-w_{i-1,j+1}+w_{i+1,j}-w_{i-1,j})}{4} \\ &-\frac{\eta_{i,j-\frac{1}{2}}(w_{i+1,j}-w_{i-1,j}+w_{i+1,j-1}-w_{i-1,j-1})}{4}], \end{aligned} \tag{4.2.20}$$

$$\begin{aligned} &[1+\frac{\Delta t}{2h^2\mathbf{Re}}(\frac{r_{i+\frac{1}{2}}\eta_{i+\frac{1}{2},j}+r_{i-\frac{1}{2}}\eta_{i-\frac{1}{2},j}}{r_i}+2\eta_{i,j+\frac{1}{2}}+2\eta_{i,j-\frac{1}{2}})]w^*_{i,j} = {s_2}^n \\ &+\frac{\Delta t}{2h^2\mathbf{Re}}(\frac{r_{i+\frac{1}{2}}\eta_{i+\frac{1}{2},j}(u_{i+1,j+1}-u_{i+1,j-1}+u_{i,j+1}-u_{i,j-1})}{4r_i} \\ &-\frac{r_{i-\frac{1}{2}}\eta_{i-\frac{1}{2},j}(u_{i,j+1}-u_{i,j-1}+u_{i-1,j+1}-u_{i-1,j-1})}{4r_i} \\ &+\frac{r_{i+\frac{1}{2}}\eta_{i+\frac{1}{2},j}w_{i+1,j}+r_{i-\frac{1}{2}}\eta_{i-\frac{1}{2},j}w_{i-1,j}}{r_i}+2\eta_{i,j+\frac{1}{2}}w_{i,j+1}+2\eta_{i,j-\frac{1}{2}}w_{i,j-1}). \end{aligned} \tag{4.2.21}$$

We use Eqs. (4.2.20) and (4.2.21) in the relaxation step in the multigrid solver.

2.B Advection Term

The advection term $(\mathbf{u}\cdot\nabla)\mathbf{u}$ in (4.2.14) is computed at cell edges using a predictor-corrector method based on unsplit second-order Godunov method developed by Collela [38], which is incorporated into the projection method [15].

Predictor Step

The predictor step is similar to 3D case, so see the Chapter 5.

Corrected Step : MAC Projection

The normal edge velocities $u^{n+\frac{1}{2}}_{i+\frac{1}{2},j}$ and $w^{n+\frac{1}{2}}_{i,j+\frac{1}{2}}$ are not in general divergence free. To remove this, modification of these edge velocities by MAC projection has been proposed in [16].

The equation

$$D^{MAC}\mathbf{G}^{MAC}p^{MAC} = D^{MAC}\mathbf{u}^{n+\frac{1}{2}} \tag{4.2.22}$$

is solved for p^{MAC} which is defined at cell centers, where

$$(D^{MAC}\mathbf{u})_{ij} = \frac{r_{i+\frac{1}{2}}u_{i+\frac{1}{2},j} - r_{i-\frac{1}{2}}u_{i-\frac{1}{2},j}}{r_i\Delta r} + \frac{w_{i,j+\frac{1}{2}} - w_{i,j-\frac{1}{2}}}{\Delta z} \tag{4.2.23}$$

and $\mathbf{G}^{MAC} = (G^{MAC}_r, G^{MAC}_z)$ is defined by

$$(G^{MAC}_r p^{MAC})_{i+\frac{1}{2},j} = \frac{p^{MAC}_{i+1,j} - p^{MAC}_{ij}}{\Delta r} \tag{4.2.24}$$

$$(G^{MAC}_z p^{MAC})_{i,j+\frac{1}{2}} = \frac{p^{MAC}_{i,j+1} - p^{MAC}_{ij}}{\Delta z}. \tag{4.2.25}$$

$D^{MAC}\mathbf{G}^{MAC}$ in (4.2.22) is simply the standard discretization of the Laplacian in the cylindrical coordinates with zero Neumann boundary conditions on physical boundaries. Equation (4.2.22) is solved by using multigrid methods.

The edge velocities are then modified to

$$u^{n+\frac{1}{2}}_{i+\frac{1}{2},j} = u^{n+\frac{1}{2}}_{i+\frac{1}{2},j} - (G^{MAC}_r p^{MAC})_{i+\frac{1}{2},j} \tag{4.2.26}$$

$$w^{n+\frac{1}{2}}_{i,j+\frac{1}{2}} = w^{n+\frac{1}{2}}_{i,j+\frac{1}{2}} - (G^{MAC}_z p^{MAC})_{i,j+\frac{1}{2}} \tag{4.2.27}$$

We can define the advection term $\mathbf{u}\cdot\nabla\mathbf{u}$ by

$$\begin{aligned}(\mathbf{u}\cdot\nabla\mathbf{u})_{ij} &= \frac{1}{2r_i}(r_{i+\frac{1}{2}}u_{i+\frac{1}{2},j} + r_{i-\frac{1}{2}}u_{i-\frac{1}{2},j})\frac{\mathbf{u}_{i+\frac{1}{2},j} - \mathbf{u}_{i-\frac{1}{2},j}}{\Delta r} \\ &+ \frac{1}{2}(w_{i,j+\frac{1}{2}} + w_{i,j-\frac{1}{2}})\frac{\mathbf{u}_{i,j+\frac{1}{2}} - \mathbf{u}_{i,j-\frac{1}{2}}}{\Delta z},\end{aligned} \tag{4.2.28}$$

and similarly for $\mathbf{u} \cdot \nabla c$, where superscript $n + \frac{1}{2}$ is again suppressed.

2.C Discretization of the projection

Our numerical solutions are constant on each cell, and the approximate projection [6] uses the the rectangular finite elements to represent the approximate solutions internally on each cell. The pressure is computed in the space S^h of functions that are bilinear in each cell and the velocity space $\mathbf{V}^h$ is the space of functions that are piecewise constant in r and linear in z in each cell for u, with a reverse form for w.

A vector field $\mathbf{v}$ is defined to be weakly divergence-free if

$$\int_\Omega \mathbf{v} \cdot \nabla \psi \, d\mathbf{x} = 0, \tag{4.2.29}$$

for each function $\psi(r, z) \in S^h$, where $d\mathbf{x} = rdrdz$.

In finding a numerical solution in terms of cell averages, we use the following two decompositions of $\mathbf{V}^h$. The first is the orthogonal decomposition in L^2 of $\mathbf{V}^h$ into the space $\overline{\mathbf{V}^h}$of cell averages and the space $\mathbf{V}^{h\perp}$ of orthogonal linear variations. That is, for a given vector field $\mathbf{v}$, we define $\overline{\mathbf{v}}$ to be the cell average on that cell when it is restricted to a cell, and define $\mathbf{v}^\perp = \mathbf{v} - \overline{\mathbf{v}}$.

The second decomposition is the projection of $\mathbf{V}^h$ onto the space of weakly divergent vector fields and that of gradients of scalar fields in S^h. So given a vector field $\mathbf{v}$, we find a scalar field $\phi \in S^h$ by solving

$$\int_\Omega \nabla\phi \cdot \nabla\psi_{i+\frac{1}{2},j+\frac{1}{2}} \, d\mathbf{x} = \int_\Omega \mathbf{v} \cdot \nabla\psi_{i+\frac{1}{2},j+\frac{1}{2}} \, d\mathbf{x} \tag{4.2.30}$$

for

$$\phi = \sum_{ij} \phi_{i+\frac{1}{2},j+\frac{1}{2}} \psi_{i+\frac{1}{2},j+\frac{1}{2}}(r, z),$$

where $\psi_{i+\frac{1}{2},j+\frac{1}{2}}$ are basis functions for S^h. Then

$$\mathbf{v}^d = \mathbf{v} - \nabla\phi \tag{4.2.31}$$

is the weakly divergence-free vector field for $\mathbf{v}$.

The approximate projection is defined by

$$\overline{\mathbf{v}^d} = \overline{\mathbf{v}} - \overline{\nabla\phi}. \tag{4.2.32}$$

The approximate projection is not usually weakly divergence-free.

In our projection method,

$$\begin{aligned} \mathbf{v} &= \overline{\mathbf{v}} = \frac{\mathbf{u}^* - \mathbf{u}^n}{\Delta t}, \\ \phi &= p^{n+\frac{1}{2}} - p^{n-\frac{1}{2}}, \\ \overline{\mathbf{v}^d} &= \frac{\mathbf{u}^{n+1} - \mathbf{u}^n}{\Delta t}. \end{aligned}$$

The linear system in (4.2.30) is solved using multigrid methods.

In this section we present a numerical method for the concentration equation (4.2.16). We will write it as the Cahn-Hilliard equation with a source term s

$$c_t = \frac{1}{\mathbf{Pe}} \nabla \cdot (M(c) \nabla \mu) + s, \tag{4.2.33}$$

$$\mu = f(c) - \mathbf{C} \Delta c, \tag{4.2.34}$$

where $s = -\nabla \cdot (c\mathbf{u})$.

We want to construct a finite difference scheme for the axisymmetric Cahn-Hilliard equation which is second-order accurate in space and time, and which conserves the mass. Following [53], we consider the following Crank-Nicholson time-stepping as the temporal and centered difference discretization of (4.2.33) and (4.2.34):

$$\frac{c_{ij}^{n+1} - c_{ij}^n}{\Delta t} = \frac{1}{\mathbf{Pe}} \tilde{\nabla}_d^e \cdot [M(c^{n+\frac{1}{2}}) \nabla_d^e \mu_{ij}^{n+\frac{1}{2}}] + s_{ij}^{n+\frac{1}{2}}, \tag{4.2.35}$$

$$\mu_{ij}^{n+\frac{1}{2}} = \frac{1}{2}(f(c_{ij}^{n+1}) + f(c_{ij}^n)) - \frac{\mathbf{C}}{2}(\Delta_d c_{ij}^{n+1} + \Delta_d c_{ij}^n), \tag{4.2.36}$$

where $f(c_{ij}^n) = \frac{dF}{dc}(c_{ij}^n)$. The choice of $f(c_{ij}^{n+1})$ in (4.2.36) makes the fully-discrete scheme (4.2.35) and (4.2.36) second-order accurate in time and allows it to have a discrete equivalent of the Lyapunov functional for the Cahn-Hilliard equation when the source term is absent.

In (4.2.35) $s_{ij}^{n+\frac{1}{2}}$ is computed by using the values $c_{ij}^{n+\frac{1}{2}}$ and $\mathbf{u}_{ij}^{n+\frac{1}{2}}$, which are computed explicitly using the methods. So (4.2.35) and (4.2.36) is a nonlinear system of two equations for c_{ij}^{n+1} and $\mu_{ij}^{n+\frac{1}{2}}$ and the nonlinearity arises from $f(c_{ij}^{n+1})$.

4.3 Discretization of axisymmetric Cahn-Hilliard equation with degenerate mobility

Let us rewrite equations (4.2.35), (4.2.36) as follows.

$$\mathbf{NSO}(c^{n+1}, \mu^{n+\frac{1}{2}}) = (f^n, g^n),$$

where

$$\mathbf{NSO}(c^{n+1},\mu^{n+\frac{1}{2}}) = (\frac{c_{ij}^{n+1}}{\Delta t} - \tilde{\nabla}_d^e \cdot [M(c_{ij})^{n+\frac{1}{2}} \nabla_d^e \mu_{ij}^{n+\frac{1}{2}}], \mu_{ij}^{n+\frac{1}{2}} - \frac{1}{2} f(c_{ij}^{n+1}) + \frac{\epsilon^2}{2}\Delta_d c_{ij}^{n+1}),$$

and the source term is

$$(f^n,\ g^n) = (\frac{c_{ij}^n}{\Delta t} + s_{ij}^{n+\frac{1}{2}},\ \frac{1}{2} f(c_{ij}^n) - \frac{\epsilon^2}{2}\Delta_d c_{ij}^n).$$

Let's discretize Eq. (4.2.35) to get a smooth operator.

$$\frac{c_{ij}^{n+1} - c_{ij}^n}{\Delta t} = \frac{1}{\mathbf{Pe}} \nabla \cdot [M(c_{ij}^{n+\frac{1}{2}}) \nabla \mu_{ij}^{n+\frac{1}{2}}] + s_{ij}^{n+\frac{1}{2}},$$

$$\frac{c_{ij}^{n+1}}{\Delta t} - \frac{1}{\mathbf{Pe}} \nabla \cdot [M(c_{ij}^{n+\frac{1}{2}}) \nabla \mu_{ij}^{n+\frac{1}{2}}] = \frac{c_{ij}^n}{\Delta t} + s_{ij}^{n+\frac{1}{2}},$$

$$\frac{c_{ij}^{n+1}}{\Delta t} - \frac{1}{\mathbf{Pe}} \left[\frac{r_{i+\frac{1}{2},j} M(c_{i+\frac{1}{2},j}^{n+\frac{1}{2}})(\mu_{i+1,j}^{n+\frac{1}{2}} - \mu_{ij}^{n+\frac{1}{2}}) - r_{i-\frac{1}{2},j} M(c_{i-\frac{1}{2},j}^{n+\frac{1}{2}})(\mu_{ij}^{n+\frac{1}{2}} - \mu_{i-1,j}^{n+\frac{1}{2}})}{r_{ij}\Delta r^2} \right.$$

$$\left. + \frac{M(c_{i,j+\frac{1}{2}}^{n+\frac{1}{2}})(\mu_{i,j+1}^{n+\frac{1}{2}} - \mu_{ij}^{n+\frac{1}{2}}) - M(c_{i,j-\frac{1}{2}}^{n+\frac{1}{2}})(\mu_{ij}^{n+\frac{1}{2}} - \mu_{i,j-1}^{n+\frac{1}{2}})}{\Delta z^2} \right] = \frac{c_{ij}^n}{\Delta t} + s_{ij}^{n+\frac{1}{2}},$$

$$\frac{c_{ij}^{n+1}}{\Delta t} + \frac{1}{\mathbf{Pe}} \left[\frac{r_{i+\frac{1}{2},j} M(c_{i+\frac{1}{2},j}^{n+\frac{1}{2}}) + r_{i-\frac{1}{2},j} M(c_{i-\frac{1}{2},j}^{n+\frac{1}{2}})}{r_{ij}\Delta r^2} + \frac{M(c_{i,j+\frac{1}{2}}^{n+\frac{1}{2}}) + M(c_{i,j-\frac{1}{2}}^{n+\frac{1}{2}})}{\Delta z^2} \right] \mu_{ij}^{n+\frac{1}{2}} \quad (4.3.37)$$

$$= \frac{c_{ij}^n}{\Delta t} + s_{ij}^{n+\frac{1}{2}} + \frac{1}{\mathbf{Pe}} \left[\frac{r_{i+\frac{1}{2},j} M(c_{i+\frac{1}{2},j}^{n+\frac{1}{2}}) \mu_{i+1,j}^{n+\frac{1}{2}} + r_{i-\frac{1}{2},j} M(c_{i-\frac{1}{2},j}^{n+\frac{1}{2}}) \mu_{i-1,j}^{n+\frac{1}{2}}}{r_{ij}\Delta r^2} \right.$$

$$\left. + \frac{M(c_{i,j+\frac{1}{2}}^{n+\frac{1}{2}}) \mu_{i,j+1}^{n+\frac{1}{2}} + M(c_{i,j-\frac{1}{2}}^{n+\frac{1}{2}}) \mu_{i,j-1}^{n+\frac{1}{2}}}{\Delta z^2} \right].$$

Next, let's discretize Eq. (4.2.36).

$$\mu_{ij}^{n+\frac{1}{2}} - \frac{1}{2} f(c_{ij}^{n+1}) + \frac{1}{2}\mathbf{C}\Delta_d c_{ij}^{n+1} = \frac{1}{2} f(c_{ij}^n) - \frac{1}{2}\mathbf{C}\Delta_d c_{ij}^n,$$

$$\mu_{ij}^{n+\frac{1}{2}} - \frac{1}{2} f(c_{ij}^m) - \frac{1}{2}\frac{\partial f(c_{ij}^m)}{\partial c}(c_{ij}^{n+1} - c_{ij}^m) + \frac{\mathbf{C}}{2}[\frac{r_{i+\frac{1}{2},j}(c_{i+1,j}^{n+1} - c_{ij}^{n+1}) - r_{i-\frac{1}{2},j}(c_{ij}^{n+1} - c_{i-1,j}^{n+1})}{r_{ij}\Delta r^2}$$

$$+ \frac{c_{i,j+1}^{n+1} - 2c_{ij}^{n+1} + c_{i,j-1}^{n+1}}{\Delta z^2}] = \frac{1}{2} f(c_{ij}^n) - \frac{1}{2}\mathbf{C}\Delta_d c_{ij}^n,$$

$$-\frac{1}{2}[\frac{\partial f(c_{ij}^m)}{\partial c} + \mathbf{C}(\frac{r_{i+\frac{1}{2},j} + r_{i-\frac{1}{2},j}}{r_{ij}\Delta r^2} + \frac{2}{\Delta z^2})]c_{ij}^{n+1} + \mu_{ij}^{n+\frac{1}{2}} = \frac{1}{2} f(c_{ij}^n) - \frac{1}{2}\mathbf{C}\Delta_d c_{ij}^n \quad (4.3.38)$$

$$+\frac{1}{2} f(c_{ij}^m) - \frac{1}{2}\frac{\partial f(c_{ij}^m)}{\partial c} c_{ij}^m - \frac{\mathbf{C}}{2}[\frac{r_{i+\frac{1}{2},j} c_{i+1,j}^m + r_{i-\frac{1}{2},j} c_{i-1,j}^{n+1}}{r_{ij}\Delta r^2} + \frac{c_{i,j+1}^m + c_{i,j-1}^{n+1}}{\Delta z^2}].$$

We use discrete Eqs. (4.3.37) and (4.3.38) in the smoothing step in multigrid method.

3.A Cell-centered Restriction and Prolongation

Definition of the restriction operator is based on the integral relation between the coarse and fine grids. Let $h = \Delta r = \Delta z$ and let $[r_i^c - h, r_i^c + h] \times [z_j^c - k, z_j^c + k]$ be a cell in the coarse grid $\Omega_{2h,2k}$ which is divided into four cells

$$[r_{2i-1}^f - \frac{h}{2},\ r_{2i-1}^f + \frac{h}{2}] \times [z_{2j-1}^f - \frac{k}{2},\ z_{2j-1}^f + \frac{k}{2}],$$

$$[r_{2i-1}^f - \frac{h}{2},\ r_{2i-1}^f + \frac{h}{2}] \times [z_{2j}^f - \frac{k}{2},\ z_{2j}^f + \frac{k}{2}],$$

$$[r_{2i}^f - \frac{h}{2},\ r_{2i}^f + \frac{h}{2}] \times [z_{2j-1}^f - \frac{k}{2},\ z_{2j-1}^f + \frac{k}{2}],$$

$$[r_{2i}^f - \frac{h}{2},\ r_{2i}^f + \frac{h}{2}] \times [z_{2j}^f - \frac{k}{2},\ z_{2j}^f + \frac{k}{2}]$$

in the fine grid $\Omega_{h,k}$. Here c and f represents the coarse and fine grids. Then the restriction $\mathcal{R}_f^c$ from $\Omega_{h,k}$ to $\Omega_{2h,2k}$ is defined by

$$\begin{aligned}
u_{ij}^c &= \frac{1}{r_i^c(2h)(2k)} \int_{z_j^c-k}^{z_j^c+k} \int_{r_i^c-h}^{r_i^c+h} u(r,z) r dr dz \\
&= \frac{1}{r_i^c(2h)(2k)} [\int_{z_{2j-1}^f-\frac{k}{2}}^{z_{2j-1}^f+\frac{k}{2}} \int_{r_{2i-1}^f-\frac{h}{2}}^{r_{2i-1}^f+\frac{h}{2}} + \int_{z_{2j}^f-\frac{k}{2}}^{z_{2j}^f+\frac{k}{2}} \int_{r_{2i-1}^f-\frac{h}{2}}^{r_{2i-1}^f+\frac{h}{2}} \\
&\quad + \int_{z_{2j-1}^f-\frac{k}{2}}^{z_{2j-1}^f+\frac{k}{2}} \int_{r_{2i}^f-\frac{h}{2}}^{r_{2i}^f+\frac{h}{2}} + \int_{z_{2j}^f-\frac{k}{2}}^{z_{2j}^f+\frac{k}{2}} \int_{r_{2i}^f-\frac{h}{2}}^{r_{2i}^f+\frac{h}{2}} u(r,z) r dr dz] \\
&= \frac{1}{4r_i^c}(r_{2i-1}^f(u_{2i-1,2j-1}^f + u_{2i-1,2j}^f) + r_{2i}^f(u_{2i,2j-1}^f + u_{2i,2j}^f)) \qquad (4.3.39)
\end{aligned}$$

Then the prolongation operator $\mathcal{P}_c^f$ from $\Omega_{2h,2k}$ to $\Omega_{h,k}$ is defined by

$$\begin{bmatrix} u_{2i-1,2j-1}^f \\ u_{2i-1,2j}^f \\ u_{2i,2j-1}^f \\ u_{2i,2j}^f \end{bmatrix} = \begin{bmatrix} \frac{r_i^c}{r_{2i-1}^f} \\ \frac{r_i^c}{r_{2i-1}^f} \\ \frac{r_i^c}{r_{2i}^f} \\ \frac{r_i^c}{r_{2i}^f} \end{bmatrix} u_{ij}^c.$$

3.B Cell-cornered Restriction and Prolongation

This is necessary when we solve the pressure in the approximate projection. In this case the coarse grid is a subgrid of the fine grid and construction of the restriction and prolongation operators are based on the following. For a numerical approximation $p_{r_{iphf},z_{jphf}}$ given at cell corners (r_{iphf}, z_{jphf}), we construct a piecewise constant function $p(r,z)$ whose value on the rectangle $(r_i, r_{i+1}) \times (z_j, z_{j+1})$ is $p_{r_{iphf},z_{jphf}}$.

We use the same notation $\Omega_{h,k}$ and $\Omega_{2h,2k}$ for a fine grid and the next level coarse grid, and $\mathcal{R}_f^c$ and $\mathcal{P}_c^f$ for restriction and prolongation operators.

Then the restriction from $\Omega_{h,k}$ to $\Omega_{2h,2k}$ is defined by

$$
\begin{aligned}
p^c_{r_{i+\frac{1}{2}},z_{j+\frac{1}{2}}} &= \frac{1}{r^c_{i+\frac{1}{2}}(2h)(2k)} \int_{z^c_{j+\frac{1}{2}}-k}^{z^c_{j+\frac{1}{2}}+k} \int_{r^c_{i+\frac{1}{2}}-h}^{r^c_{i+\frac{1}{2}}+h} p\, r dr dz \\
&= \frac{1}{r^c_{i+\frac{1}{2}}(2h)(2k)} \\
&\quad \Big[\int_{z^f_{2j-\frac{1}{2}}}^{z^f_{2j-\frac{1}{2}}+\frac{k}{2}} \int_{r^f_{2i-\frac{1}{2}}}^{r^f_{2i-\frac{1}{2}}+\frac{h}{2}} + \int_{z^f_{2j-\frac{1}{2}}}^{z^f_{2j-\frac{1}{2}}+\frac{k}{2}} \int_{r^f_{2i+\frac{1}{2}}-\frac{h}{2}}^{r^f_{2i+\frac{1}{2}}+\frac{h}{2}} + \int_{z^f_{2j-\frac{1}{2}}}^{z^f_{2j-\frac{1}{2}}+\frac{k}{2}} \int_{r^f_{2i+\frac{3}{2}}-\frac{h}{2}}^{r^f_{2i+\frac{3}{2}}} \\
&\quad \Big[\int_{z^f_{2j+\frac{1}{2}}-\frac{k}{2}}^{z^f_{2j+\frac{1}{2}}+\frac{k}{2}} \int_{r^f_{2i-\frac{1}{2}}}^{r^f_{2i-\frac{1}{2}}+\frac{h}{2}} + \int_{z^f_{2j+\frac{1}{2}}-\frac{k}{2}}^{z^f_{2j+\frac{1}{2}}+\frac{k}{2}} \int_{r^f_{2i+\frac{1}{2}}-\frac{h}{2}}^{r^f_{2i+\frac{1}{2}}+\frac{h}{2}} + \int_{z^f_{2j+\frac{1}{2}}-\frac{k}{2}}^{z^f_{2j+\frac{1}{2}}+\frac{k}{2}} \int_{r^f_{2i+\frac{3}{2}}-\frac{h}{2}}^{r^f_{2i+\frac{3}{2}}} \\
&\quad + \int_{z^f_{2j+\frac{3}{2}}-\frac{k}{2}}^{z^f_{2j+\frac{3}{2}}} \int_{r^f_{2i-\frac{1}{2}}}^{r^f_{2i-\frac{1}{2}}+\frac{h}{2}} + \int_{z^f_{2j+\frac{3}{2}}-\frac{k}{2}}^{z^f_{2j+\frac{3}{2}}} \int_{r^f_{2i+\frac{1}{2}}-\frac{h}{2}}^{r^f_{2i+\frac{1}{2}}+\frac{h}{2}} + \int_{z^f_{2j+\frac{3}{2}}-\frac{k}{2}}^{z^f_{2j+\frac{3}{2}}} \int_{r^f_{2i+\frac{3}{2}}-\frac{h}{2}}^{r^f_{2i+\frac{3}{2}}} p\, r dr dz
\end{aligned}
$$

3.C Standard Basis Function $\psi_{i+\frac{1}{2},j+\frac{1}{2}}$ for S^h

The standard basis function $\psi_{i+\frac{1}{2},j+\frac{1}{2}}$ for S^h is a piecewise bilinear function which satisfies

$$\psi_{i+\frac{1}{2},j+\frac{1}{2}}(r_{k+\frac{1}{2}}, z_{l+\frac{1}{2}}) = \delta_{ik}\delta_{jl}$$

In the case when $(r_{i+\frac{1}{2}}, z_{j+\frac{1}{2}})$ is in the interior, $\psi_{i+\frac{1}{2},j+\frac{1}{2}}$ has a support in cells (i,j), $(i+1,j)$, $(i,j+1)$ and $(i+1,j+1)$.

$$
\psi_{i+\frac{1}{2},j+\frac{1}{2}}(r,z) = \begin{cases}
\frac{r-r_{i-\frac{1}{2}}}{\Delta r}\frac{z-z_{j-\frac{1}{2}}}{\Delta z} & \text{on cell } (i,j) \\
-\frac{r-r_{i+\frac{3}{2}}}{\Delta r}\frac{z-z_{j-\frac{1}{2}}}{\Delta z} & \text{on cell } (i+1,j) \\
-\frac{r-r_{i-\frac{1}{2}}}{\Delta r}\frac{z-z_{j+\frac{3}{2}}}{\Delta z} & \text{on cell } (i,j+1) \\
\frac{r-r_{i+\frac{3}{2}}}{\Delta r}\frac{z-z_{j+\frac{3}{2}}}{\Delta z} & \text{on cell } (i+1,j+1)
\end{cases}
$$

$$\nabla\psi_{i+\frac{1}{2},j+\frac{1}{2}}(r,z) = \begin{cases} (\frac{z-z_{j-\frac{1}{2}}}{\Delta r\Delta z}, \frac{r-r_{i-\frac{1}{2}}}{\Delta r\Delta z}) & \text{on cell } (i,j) \\ (-\frac{z-z_{j-\frac{1}{2}}}{\Delta r\Delta z}, -\frac{r-r_{i+\frac{3}{2}}}{\Delta r\Delta z}) & \text{on cell } (i+1,j) \\ (-\frac{z-z_{j+\frac{3}{2}}}{\Delta r\Delta z}, -\frac{r-r_{i-\frac{1}{2}}}{\Delta r\Delta z}) & \text{on cell } (i,j+1) \\ (\frac{z-z_{j+\frac{3}{2}}}{\Delta r\Delta z}, \frac{r-r_{i+\frac{3}{2}}}{\Delta r\Delta z}) & \text{on cell } (i+1,j+1) \end{cases}$$

To find a scalar field ϕ in (4.2.30) for a given vector field $\mathbf{v}$, we need to construct the stiffness matrix in (4.2.30). In evaluating the integral in (4.2.30), we assume that $\Delta r = \Delta z = h$. Then

$$\int_\Omega \nabla\psi_{k+\frac{1}{2},l+\frac{1}{2}} \cdot \nabla\psi_{i+\frac{1}{2},j+\frac{1}{2}}\, d\mathbf{x} = \begin{cases} -\frac{r_i}{3} & \text{if } (k,l) = (i-1,j-1) \\ -\frac{r_i+r_{i+1}}{6} & \text{if } (k,l) = (i,j-1) \\ -\frac{r_{i+1}}{3} & \text{if } (k,l) = (i+1,j-1) \\ -\frac{r_i}{3} & \text{if } (k,l) = (i-1,j) \\ \frac{4(r_i+r_{i+1})}{3} & \text{if } (k,l) = (i,j) \\ -\frac{r_{i+1}}{3} & \text{if } (k,l) = (i+1,j) \\ -\frac{r_i}{3} & \text{if } (k,l) = (i-1,j+1) \\ -\frac{r_i+r_{i+1}}{6} & \text{if } (k,l) = (i,j+1) \\ -\frac{r_{i+1}}{3} & \text{if } (k,l) = (i+1,j+1) \end{cases}$$

$$\begin{aligned} \int_{\Omega_{ij}} \mathbf{u}_{ij} \cdot \nabla\psi_{i+\frac{1}{2},j+\frac{1}{2}}\, d\mathbf{x} &= \int_{\Omega_{ij}} (u_{ij}, w_{ij}) \cdot (\frac{z-z_{j-\frac{1}{2}}}{\Delta r\Delta z}, \frac{r-r_{i-\frac{1}{2}}}{\Delta r\Delta z})\, d\mathbf{x} \\ &= \int_{j-\frac{1}{2}}^{j+\frac{1}{2}} \int_{i-\frac{1}{2}}^{i+\frac{1}{2}} [u_{ij}(\frac{z-z_{j-\frac{1}{2}}}{\Delta r\Delta z}) + w_{ij}(\frac{r-r_{i-\frac{1}{2}}}{\Delta r\Delta z})] r dr dz \\ &= \frac{hr_i}{2} u_{ij} + \frac{1}{12} h(h+6r_i) w_{ij} \end{aligned}$$

$$\begin{aligned}\int_{\Omega_{i+1,j}} \mathbf{u}_{i+1,j}\cdot\nabla\psi_{i+\frac{1}{2},j+\frac{1}{2}}\,d\mathbf{x} &= \int_{\Omega_{i+1,j}} (u_{i+1,j},w_{i+1,j})\cdot(-\frac{z-z_{j-\frac{1}{2}}}{\Delta r\Delta z},-\frac{r-r_{i+\frac{3}{2}}}{\Delta r\Delta z})\,d\mathbf{x}\\ &= \int_{j-\frac{1}{2}}^{j+\frac{1}{2}}\int_{i+\frac{1}{2}}^{i+\frac{3}{2}}[u_{i+1,j}(-\frac{z-z_{j-\frac{1}{2}}}{\Delta r\Delta z})+w_{i+1,j}(-\frac{r-r_{i+\frac{3}{2}}}{\Delta r\Delta z})]rdrdz\\ &= -\frac{1}{2}h(h+r_i)u_{i+1,j}+\frac{1}{12}h(5h+6r_i)w_{i+1,j}\end{aligned}$$

$$\begin{aligned}\int_{\Omega_{i,j+1}} \mathbf{u}_{i,j+1}\cdot\nabla\psi_{i+\frac{1}{2},j+\frac{1}{2}}\,d\mathbf{x} &= \int_{\Omega_{i,j+1}} (u_{i,j+1},w_{i,j+1})\cdot(-\frac{z-z_{j+\frac{3}{2}}}{\Delta r\Delta z},-\frac{r-r_{i-\frac{1}{2}}}{\Delta r\Delta z})\,d\mathbf{x}\\ &= \int_{j+\frac{1}{2}}^{j+\frac{3}{2}}\int_{i-\frac{1}{2}}^{i+\frac{1}{2}}[-u_{i,j+1}(\frac{z-z_{j+\frac{3}{2}}}{\Delta r\Delta z})-w_{i,j+1}(\frac{r-r_{i-\frac{1}{2}}}{\Delta r\Delta z})]rdrdz\\ &= \frac{hr_i}{2}u_{i,j+1}-\frac{1}{12}h(h+6r_i)w_{i,j+1}\end{aligned}$$

$$\begin{aligned}\int_{\Omega_{i+1,j+1}} \mathbf{u}_{i+1,j+1}\cdot\nabla\psi_{i+\frac{1}{2},j+\frac{1}{2}}\,d\mathbf{x} &= \int_{\Omega_{i+1,j+1}} (u_{i+1,j+1},w_{i+1,j+1})\cdot(\frac{z-z_{j+\frac{3}{2}}}{\Delta r\Delta z},\frac{r-r_{i+\frac{3}{2}}}{\Delta r\Delta z})\,d\mathbf{x}\\ &= \int_{j+\frac{1}{2}}^{j+\frac{3}{2}}\int_{i+\frac{1}{2}}^{i+\frac{3}{2}}[u_{i+1,j+1}(\frac{z-z_{j+\frac{3}{2}}}{\Delta r\Delta z})+w_{i+1,j+1}(\frac{r-r_{i+\frac{3}{2}}}{\Delta r\Delta z})]rdrdz\\ &= -\frac{1}{2}h(h+r_i)u_{i+1,j+1}-\frac{1}{12}h(5h+6r_i)w_{i+1,j+1}\end{aligned}$$

$$\begin{aligned}\int_{\Omega_{ij}} \psi_{i+\frac{1}{2},j+\frac{1}{2}}\,d\mathbf{x} &= \int_{\Omega_{ij}} \psi_{i+\frac{1}{2},j+\frac{1}{2}}\,d\mathbf{x}=\int_{j-\frac{1}{2}}^{j+\frac{1}{2}}\int_{i-\frac{1}{2}}^{i+\frac{1}{2}}\frac{r-r_{i-\frac{1}{2}}}{\Delta r}\frac{z-z_{j-\frac{1}{2}}}{\Delta z}\,d\mathbf{x}\\ &= \frac{h^2(h+6r_i)}{24},\end{aligned}$$

$$\begin{aligned}\int_{\Omega_{i+1,j}} \psi_{i+\frac{1}{2},j+\frac{1}{2}}\,d\mathbf{x} &= \int_{\Omega_{i+1,j}} \psi_{i+\frac{1}{2},j+\frac{1}{2}}\,d\mathbf{x}=\int_{j-\frac{1}{2}}^{j+\frac{1}{2}}\int_{i+\frac{1}{2}}^{i+\frac{3}{2}}(1-\frac{r-r_{i+\frac{1}{2}}}{\Delta r})\frac{z-z_{j-\frac{1}{2}}}{\Delta z}\,d\mathbf{x}\\ &= \frac{h^2(5h+6r_i)}{24},\end{aligned}$$

$$\begin{aligned}\int_{\Omega_{i,j+1}} \psi_{i+\frac{1}{2},j+\frac{1}{2}}\, d\mathbf{x} &= \int_{\Omega_{i,j+1}} \psi_{i+\frac{1}{2},j+\frac{1}{2}}\, d\mathbf{x} = \int_{j+\frac{1}{2}}^{j+\frac{3}{2}} \int_{i-\frac{1}{2}}^{i+\frac{1}{2}} \frac{r-r_{i+\frac{1}{2}}}{\Delta r}(1-\frac{z-z_{j+\frac{1}{2}}}{\Delta z})\, d\mathbf{x} \\ &= \frac{h^2(h+6r_i)}{24},\end{aligned}$$

$$\begin{aligned}\int_{\Omega_{i+1,j+1}} \psi_{i+\frac{1}{2},j+\frac{1}{2}}\, d\mathbf{x} &= \int_{\Omega_{i+1,j+1}} \psi_{i+\frac{1}{2},j+\frac{1}{2}}\, d\mathbf{x} = \int_{j+\frac{1}{2}}^{j+\frac{3}{2}} \int_{i+\frac{1}{2}}^{i+\frac{3}{2}} (1-\frac{r-r_{i+\frac{1}{2}}}{\Delta r})(1-\frac{z-z_{j+\frac{1}{2}}}{\Delta z})\, d\mathbf{x} \\ &= \frac{h^2(5h+6r_i)}{24}.\end{aligned}$$

$$\begin{aligned}\int_{\Omega} \mathbf{u}\cdot\nabla\psi_{i+\frac{1}{2},j+\frac{1}{2}}\, d\mathbf{x} &= -\frac{h}{2}(r_{i+1}(u_{i+1,j+1}+u_{i+1,j}) - r_i(u_{i,j+1}+u_{ij})) \\ &- \frac{h}{2}((r_{i+1}-\frac{h}{6})(w_{i+1,j+1}-w_{i+1,j}) + (r_i+\frac{h}{6})(w_{i,j+1}-w_{ij}))\end{aligned}$$

Then approximations of $\Delta\phi$ and $\nabla\cdot\mathbf{u}$ at $(r_{i+\frac{1}{2}}, z_{j+\frac{1}{2}})$ are defined by

$$\begin{aligned}(L\phi)_{i+\frac{1}{2},j+\frac{1}{2}} &= -\frac{\int \nabla\phi\cdot\nabla\psi_{i+\frac{1}{2},j+\frac{1}{2}}\, d\mathbf{x}}{\int \psi_{i+\frac{1}{2},j+\frac{1}{2}}\, d\mathbf{x}} \\ (D\mathbf{u})_{i+\frac{1}{2},j+\frac{1}{2}} &= -\frac{\int \mathbf{u}\cdot\nabla\psi_{i+\frac{1}{2},j+\frac{1}{2}}\, d\mathbf{x}}{\int \psi_{i+\frac{1}{2},j+\frac{1}{2}}\, d\mathbf{x}}\end{aligned}$$

4.4 Rayleigh-Instability (Linear Analysis)

In this section, we will consider a long cylindrical thread of a viscous liquid, the viscosity and density of which are denoted by η_i and ρ_i respectively, in an infinite mass of another viscous fluid of viscosity η_o and ρ_o. In the thread evolution, the deformation growth rates are consistent with the predictions of linear analysis (e.g. see Tomotika [123]) in the context of Stokes flow. In this analysis, the growth of an initially sinusoidal perturbation to the thread radius R_0, at leading order, is seen to be given by

$$R(z,t) = R_0 + \alpha(t)\cos(2\pi z/\lambda),$$

where λ is the disturbance wavelength,

$$\alpha(t) = \alpha_0 e^{\omega t} \text{ and } \omega = \sigma\Omega(x,\beta)/2R_0\eta_0,$$

where ω is the growth rate, $\beta = \eta_i/\eta_o$ is the viscosity ratio, α_0 is the amplitude of the initial perturbation, and $x = 2\pi R_0/\lambda$ is the dimensionless wavenumber. The function $\Omega(x,\beta)$ is the dimensionless

growth rate. For each viscosity ratio β, there exists a maximum growing mode x_m and a corresponding maximum nondimensional growth rate Ω_m.

$$\Omega(x,\beta) = (1 - k^2 R_o^2)\Phi(kR_o) = (1 - x^2)\Phi(x),$$

where $k = 2\pi/\lambda$ and the function $\Phi(x)$ is given by

$$\Phi(x) = \frac{N(x)}{D(x)}, \tag{4.4.40}$$

with

$$\left.\begin{aligned} N(x) &\equiv I_1(x)\Delta_1 - \{xI_0(x) - I_1(x)\}\Delta_2, \\ D(x) &\equiv (\eta_i/\eta_o)\{xI_0(x) - I_1(x)\}\Delta_1 \\ &\quad -(\eta_i/\eta_o)\{(x^2+1)I_1(x) - xI_0(x)\}\Delta_2 \\ &\quad -\{xK_0(x) + K_1(x)\}\Delta_3 \\ &\quad -\{(x_2+1)K_1(x) + xK_0(x)\}\Delta_4. \end{aligned}\right\} \tag{4.4.41}$$

In these expressions $I_n(x)$ and $K_n(x)$ are the modified Bessel functions of the nth order, Δ_1, Δ_2, Δ_3 and Δ_4 are all functions of x expressed in determinantal forms as follows:

$$\Delta_1 = \begin{vmatrix} xI_0(x) - I_1(x) & K_1(x) & -xK_0(x) - K_1(x) \\ I_0(x) + xI_1(x) & -K_0(x) & -K_0(x) + xK_1(x) \\ (\eta_i/\eta_o)xI_0(x) & K_1(x) & -xK_0(x) \end{vmatrix},$$

$$\Delta_2 = \begin{vmatrix} I_1(x) & K_1(x) & -xK_0(x) - K_1(x) \\ I_0(x) & -K_0(x) & -K_0(x) + xK_1(x) \\ (\eta_i/\eta_o)xI_1(x) & K_1(x) & -xK_0(x) \end{vmatrix},$$

$$\Delta_3 = \begin{vmatrix} I_1(x) & xI_0(x) - I_1(x) & -xK_0(x) - K_1(x) \\ I_0(x) & I_0(x) + xI_1(x) & -K_0(x) + xK_1(x) \\ (\eta_i/\eta_o)xI_1(x) & (\eta_i/\eta_o)xI_0(x) & -xK_0(x) \end{vmatrix},$$

$$\Delta_4 = \begin{vmatrix} I_1(x) & xI_0(x) - I_1(x) & K_1(x) \\ I_0(x) & I_0(x) + xI_1(x) & -K_0(x) \\ (\eta_i/\eta_o)xI_1(x) & K_1(x) & K_1(x) \end{vmatrix}.$$

Using (4.4.40) and (4.4.41) the values of the function $(1 - x^2)\Phi(x)$, to which ω is proportional, can be calculated.

As an example, consider the case in which $\eta_i/\eta_o = 0.91$. The values of $(1 - x^2)\Phi(x)$ calculated by using the preceding general formulae, putting $\eta_i/\eta_o = 0.91$, for values of x in the range of instability from $x = 0$ and $x = 1$ are shown in Table 4.1.

Table 4.1: $\eta_i/\eta_o = 0.91$

x	$(1-x^2)\Phi(x)$
0.0	0
0.1	0.1904 $\times 10^{-1}$
0.2	0.2980 $\times 10^{-1}$
0.3	0.4877 $\times 10^{-1}$
0.4	0.6373 $\times 10^{-1}$
0.5	0.7243 $\times 10^{-1}$
0.6	0.7366 $\times 10^{-1}$
0.7	0.6688 $\times 10^{-1}$
0.8	0.5210 $\times 10^{-1}$
0.9	0.2962 $\times 10^{-1}$
1.0	0 $\times 10^{-1}$

Then, the value of x of which $(1-x^2)\Phi(x)$ is a maximum, *i.e.*, the value of ka corresponding to the maximum instability has been found with the aid of Lagrange's interpolation formula. It is

$$x = kR_0 = 0.568.$$

Thus, the wave-length of the varicosity corresponding to the mode of maximum instability is found to be

$$\lambda = 5.53 \times 2R_0.$$

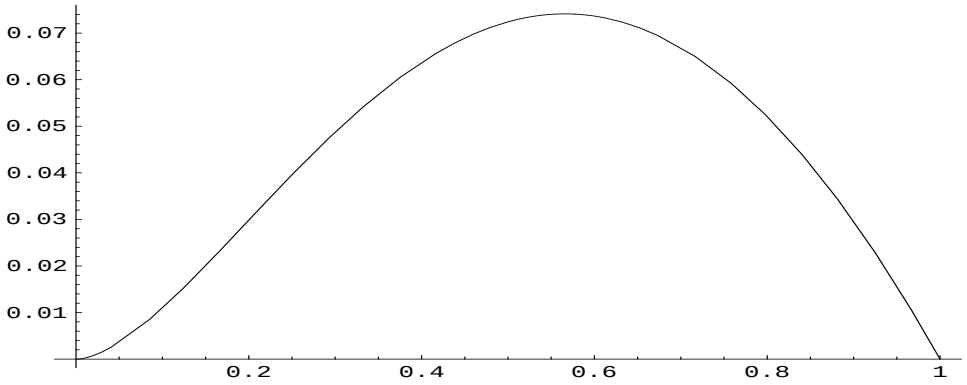

Figure 4.1: Curve of $(1-x^2)\Psi(x)$ when $\eta_i/\eta_o = 0.91$.

Fig. 1 shows the curve of $(1-x^2)\Phi(x)$ plotted against x in the present case when $\eta_i/\eta_o = 0.91$

4.A Numerical Results

Consider a thread of a neutrally buoyant Newtonian liquid with undeformed radius R_o and viscosity η_i, suspended in a bath of a second Newtonian fluid with viscosity η_o. The interfacial tension between the two fluids is σ. We assume that σ is constant. We will perform two simulations corresponding to low and moderate Reynolds numbers.

In the low Reynolds number case, we take the nondimensional numbers $R_o = 0.5,\ \alpha_o = 0.05,$ $\epsilon = 0.03,\ \eta_i/\eta_o = 0.91,\ \rho_i/\rho_o = 1.0,\ \mathbf{Re} = 0.58,\ \mathbf{We} = 0.042$. The mesh size is 64×256 and the time step is $\Delta t = 0.001$. The initial velocity is equal to zero and the initial concentration is

$$c_0(r, z) = \frac{1}{2}[1 - \tanh((r - R_o - \alpha_0 \cos(z))/(\sqrt{2}\epsilon))],$$

which represents a perturbed cylinder.

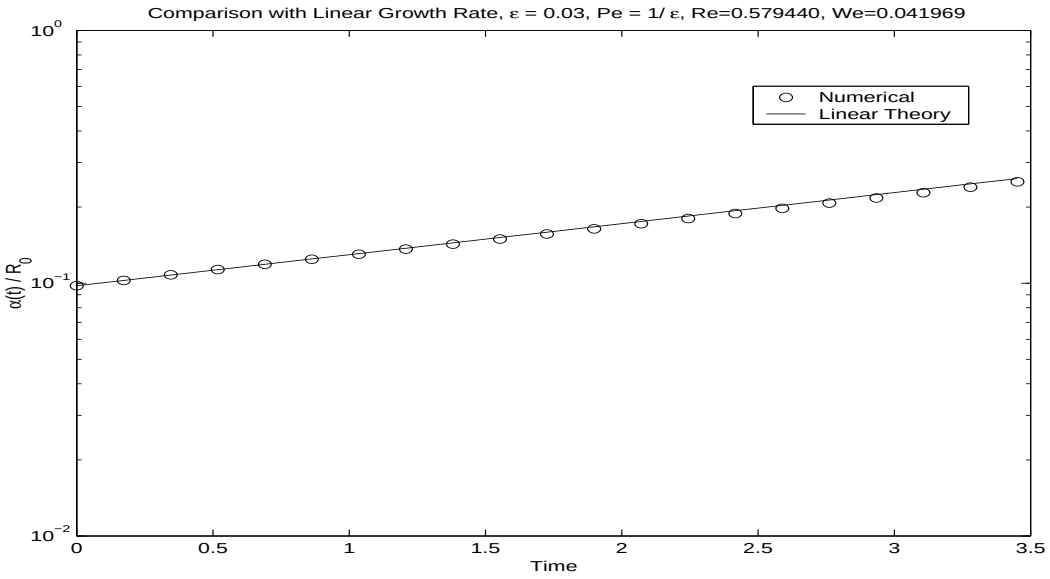

Figure 4.2: Comparison of the growth rates of the NSCH model and linear theory.

Let us compare the simulation results with linear theory. In particular, we compare the perturbation size $\alpha(t)/R_0$. The result is shown in a log-linear plot in Fig. 4.2. The linear prediction is given by the solid line and the circles correspond the numerical results. The theoretical and numerical results agree very well even up to the approximate pinchoff time $t \approx 7$.

Next, we consider pinchoff at moderate Reynolds. The physical parameters are as before except that $\mathbf{Re} = 6.0$ and $\mathbf{We} = 0.18$. The numerical parameters are the same as before with $\epsilon = 0.02$ and $\mathbf{Pe} = 1.0/\epsilon$. In Fig. 4.3, the exponential growth at early times of the numerical perturbation is shown.

Although it is not shown, the result agrees with linear theory. The full evolution of the thread is shown in Fig. 4.4. A neck develops and pinches off to form three droplets at approximately time $t = 2.5$. At this first pinchoff, there is a slight overturning of the interface in the neck region (see $t = 1.8$). At later times, the main drops circularize due to surface tension while the smaller daughter drops undergo additional pinchoff events. In each event, it is the outer most drops that pinchoff. This significantly reduces the size of the drops and eventually leads to steady state in which a distribution of small drops separates the larger ones. The small drops are nearly monodisperse in size.

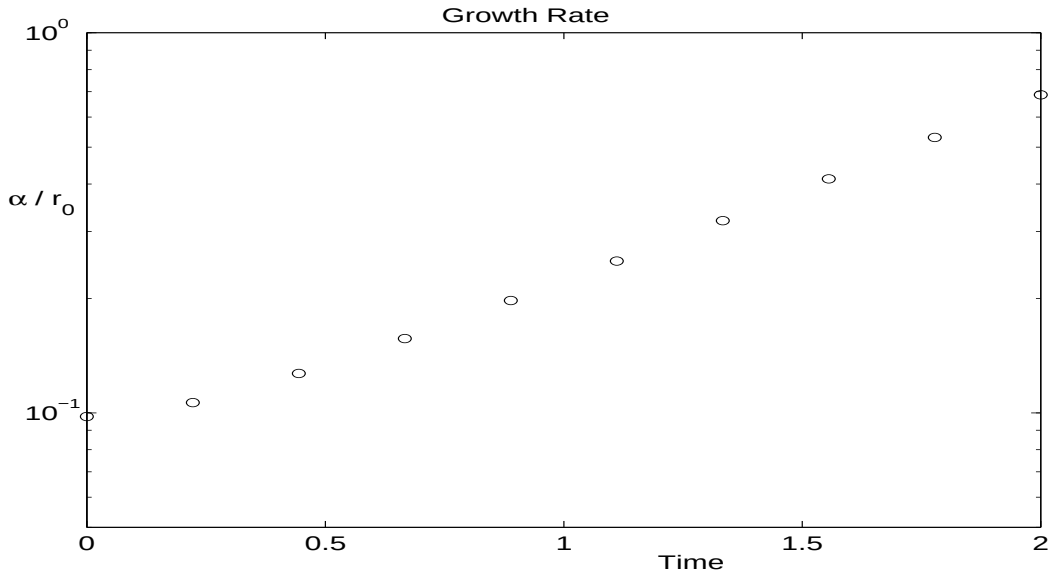

Figure 4.3: Growth rate at early times with $\mathbf{Re} = 6.0$ and $\mathbf{We} = 0.18$.

4.5 Jet pinch-off in liquid-liquid systems

5.A Experimental description and fluid properties

The experiments were performed in the closed loop facility depicted in Fig. 4.5 [98]. The tank was filled with a combination of the immiscible fluids. The upper $200\ mm$ of the tank contained the lighter, less dense fluid, while the remainder was filled with the heavier fluid. The heavier fluid was drawn from the bottom of the tank and driven through the flow loop by a magnetic-drive pump. A needle valve controlled the flow rate. The diameter of the submerged exit nozzle was $10mm$. A piston-driven forcer was used to impose a regular sinusoidal oscillation on the nozzle exit velocity.

Two fluid combinations were employed in this study. In both combinations, one fluid was a water-

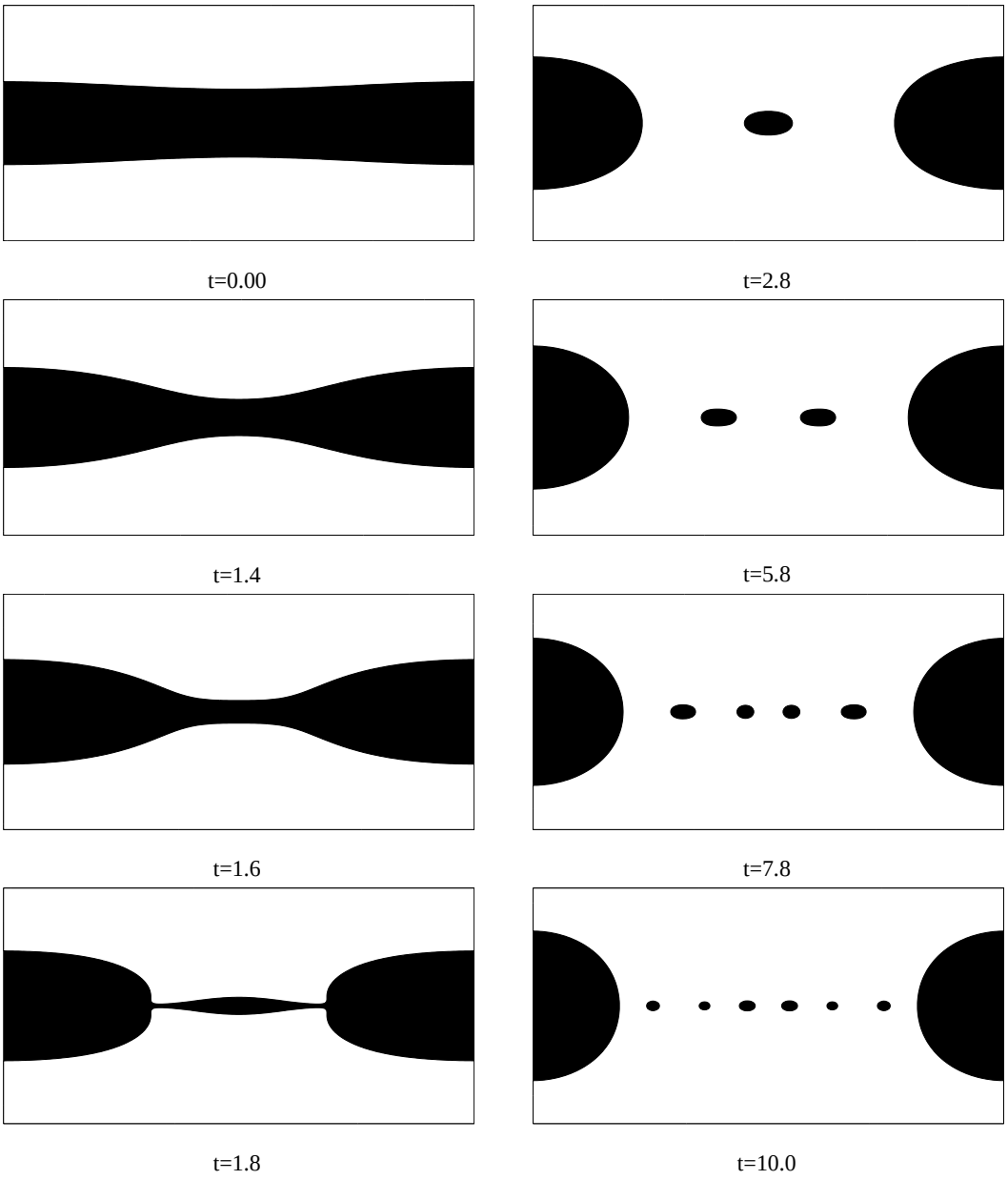

Figure 4.4: Time evolution of a thread of fluid at moderate Reynolds number. The dimensionless times are shown below each figure.

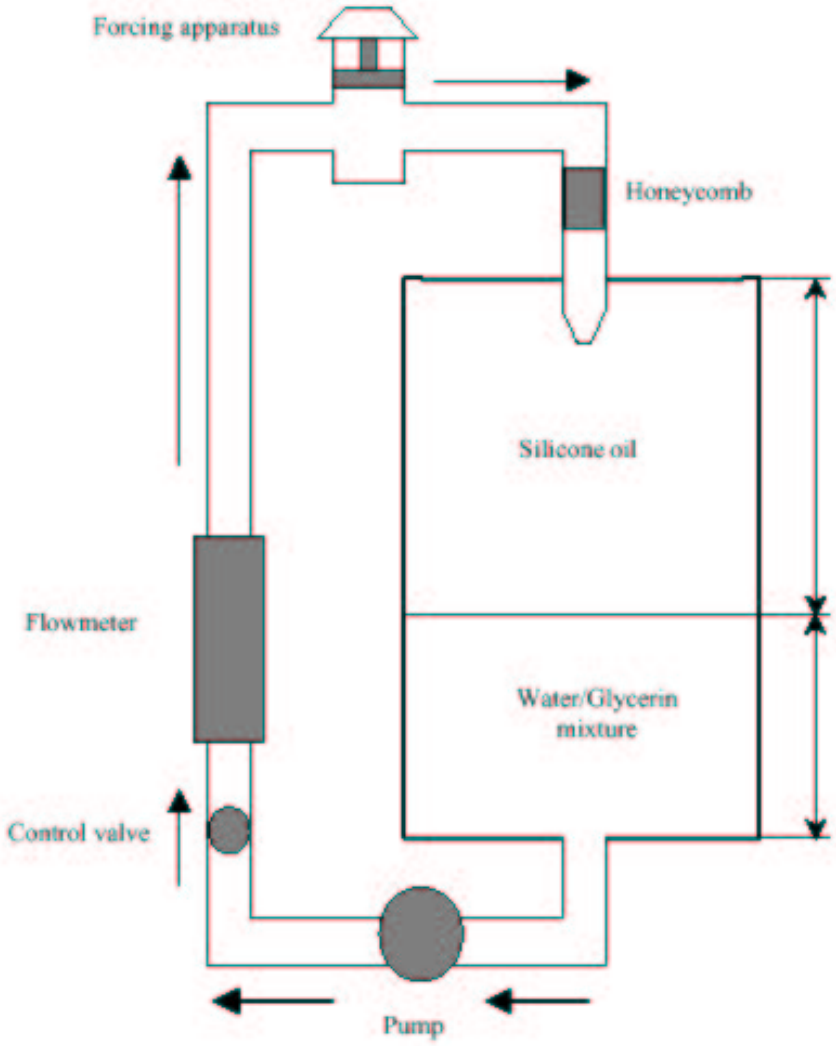

Figure 4.5: Jet flow facility (I. N. Milosevic, E. K. Longmire, “Pinch-off modes and satellite formation in liquid/liquid jet systems”, International Journal of Multiphase Flow, June 2002)

glycerin mixture, and the other was a Dow Corning 200 fluid. The fluid properties for the two combinations are shown in Table 4.2, where ρ is fluid density and μ is dynamic viscosity. The jet and ambient fluid are denoted with i and o, respectively.

Fluid Property	Density ρ (kg/m^2)	Dyn. Viscosity μ (cP)
Ambient Fluid (o) Dow Corning 200 Fluid	920	4.6
Jet Fluid (i) Water/Glycerin (52/48 percent by volume)	1136.4	8.35

Table 4.2: Fluid properties

The interfacial tension was measured to be $29mN/m$ using a spinning drop tensiometer (Joseph et al. 1992). Hence the non-dimensional Bond number, $Bo = \Delta\rho g D^2/\sigma$, was approximately 6, where $\Delta\rho$ is the density difference between fluids, g is the gravitational constant, D is the nozzle diameter, and σ is the interfacial tension.

The remaining parameters chosen to characterize the flow were the density ratio, the viscosity ratio, a Reynolds number based on the jet flow and fluid properties, a Froude number, and a Strouhal number (for forced flow):

$$\frac{\rho_i}{\rho_o},\ \frac{\mu_i}{\mu_o},\ \mathbf{Re} = \frac{\rho_i U_e D}{\mu_i},\ \mathbf{Fr} = \frac{U_e\sqrt{\rho_i}}{\sqrt{\Delta\rho g D}},\ \mathbf{St} = \frac{fD}{U_e},$$

where U_e is the jet exit velocity, and f is the forcing frequency. The Reynolds number represents the ratio of inertial to viscous forces, the Froude number represents the ratio of inertial to buoyant forces, and the Bond number represents the ratio of buoyant to interfacial tension forces. For the flow conditions chosen, the effects of inertia, gravity, and interfacial tension were all significant.

5.B Governing equations

$$\begin{aligned}
\mathbf{u}_t + \mathbf{u}\cdot\nabla\mathbf{u} &= -\nabla q + \frac{1}{\mathbf{Re}}\nabla\cdot[\eta(c)(\nabla\mathbf{u} + \nabla\mathbf{u}^T)] \qquad (4.5.42)\\
&\quad -\frac{\epsilon}{\mathbf{We}}(\Delta c\nabla c - \frac{1}{2}\nabla|\nabla c|^2) + \frac{\rho(c)}{\mathbf{Fr}^2}\mathbf{G},\\
\nabla\cdot\mathbf{u} &= 0, \qquad (4.5.43)\\
c_t + \nabla\cdot(c\mathbf{u}) &= \frac{1}{\mathbf{Pe}}\nabla\cdot(M(c)\nabla\mu), \qquad (4.5.44)\\
\mu &= f(c) - \mathbf{C}\Delta c, \qquad (4.5.45)
\end{aligned}$$

$$\frac{\rho_i}{\rho_o} = 1.235, \;\; \frac{\mu_i}{\mu_o} = 1.591, \;\; \mathbf{Re} = \frac{\rho_i U_e D}{\mu_i} = 58.031, \;\; \mathbf{Fr} = \frac{U_e\sqrt{\rho_i}}{\sqrt{\Delta\rho g D}} = 0.274,$$

$$\epsilon = 0.02, \;\; \mathbf{St} = \frac{fD}{U_e} = 3.478, \;\; \mathbf{We} = 0.538, \;\; \mathbf{Pe} = 0.02/\epsilon.$$

We take 64×512 for space mesh and $\Delta t = 1 \times 10^{-3}$. And for the initial concentration profile, we choose a cylinder column.

$$c(r, z) = 0.5(1 - \tanh(\frac{r - 0.5}{4\epsilon}))$$

Inflow boundary condition

$$w(r, 2\pi) = -(0.5 + 0.25\sin(2\pi t\mathbf{St}))(1 - \tanh(\frac{r - 0.5}{4\epsilon})), \;\; u(r, 2\pi) = 0.$$

5.C Results

The very sharp jet tip and nearly flat upstream end of the drop characterize the interface shape just before pinch-off in Fig. 4.6 [98]. And the numerical simulation shows similar shape in Fig. 4.11.

Analogous qualitative agreement is obtained between the experimental and numerical axial velocity and vorticity as seen in Figs. (4.16)-(4.17) and (4.20)-(4.21) and (4.18)-(4.19) and (4.22)-(4.23), respectively. In both the experiments and the numerics prior to pinchoff, the maximum axial velocity is located approximately at the jet neck. The fluid is thus accelerating into the neck and acting to increase the volume of the drop. Further, on each side of the symmetry line, two centers of vorticity are seen: one near the jet neck (corresponding to the maximum in axial velocity) and one along the upstream side of the developing droplet associated with variations in the curvature of the interface. This latter vorticity rotates and flattens the upstream side of the drop enhancing pinchoff. Also note that the vorticity is primarily concentrated in the silicone oil outside the jet. This is due to the fact that in this experiment and simulation, the water-glycerine (jet) mixture is more viscous than the silicone oil (ambient). After pinchoff, the maximum axial velocity is located approximately at the upstream of the drop and the vorticity centers also remain near the upstream side of the drop.

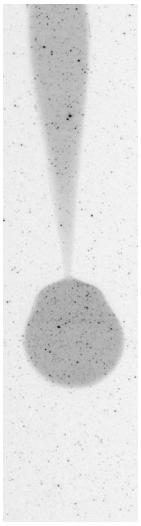

Figure 4.6:

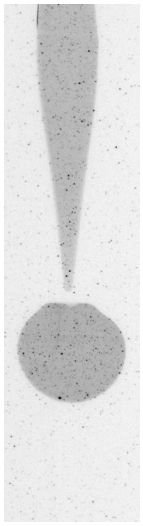

Figure 4.7:

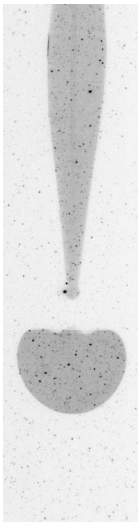

Figure 4.8:

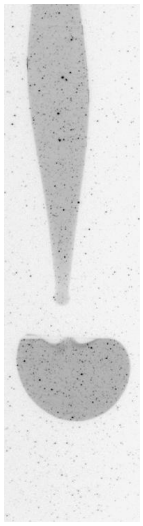

Figure 4.9:

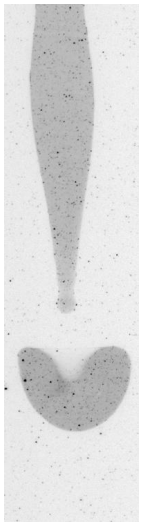

Figure 4.10:

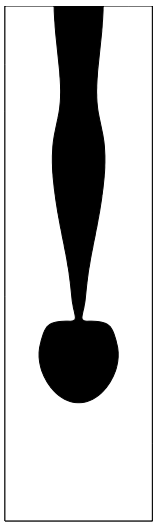

Figure 4.11:

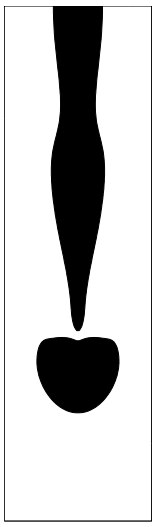

Figure 4.12:

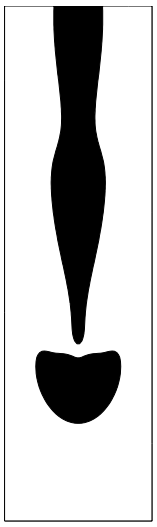

Figure 4.13:

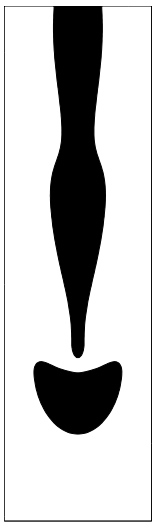

Figure 4.14:

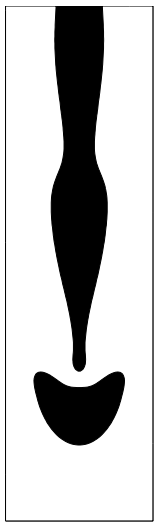

Figure 4.15:

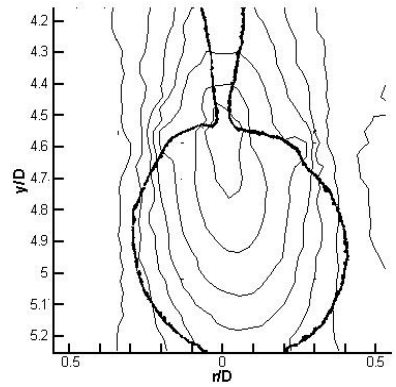

Figure 4.16: Normalized axial velocity contour of forced flow at $St = 3.3$ and $Re = 58$.

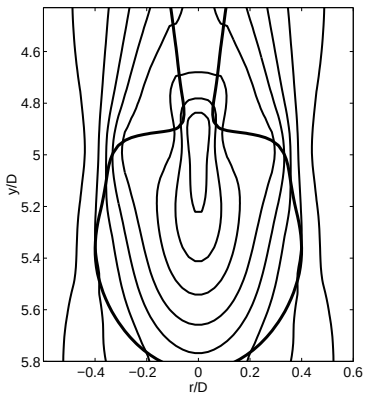

Figure 4.17: Simulation

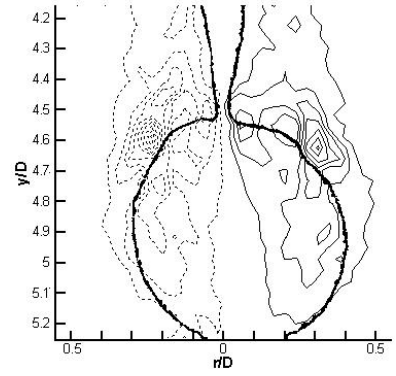

Figure 4.18: Normalized vorticity fields of forced flow at $St = 3.3$ and $Re = 58$.

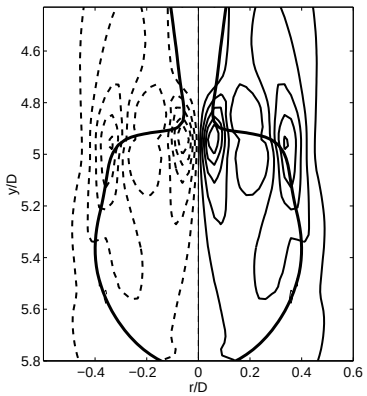

Figure 4.19: Simulation.

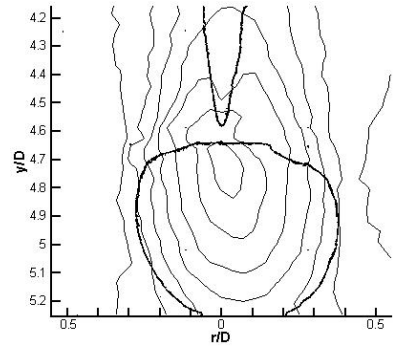

Figure 4.20: Normalized axial velocity contour of forced flow at $St = 3.3$ and $Re = 58$.

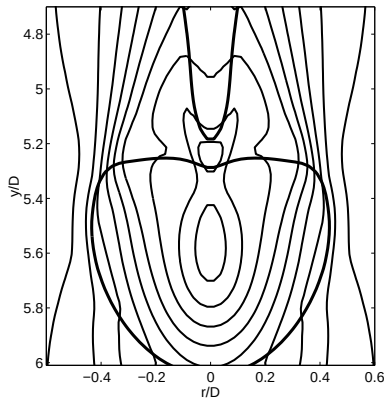

Figure 4.21: Simulation.

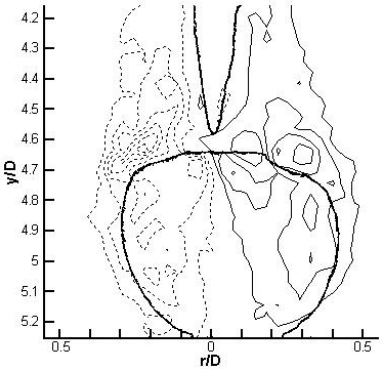

Figure 4.22: Normalized vorticity fields of forced flow at $St = 3.3$ and $Re = 58$.

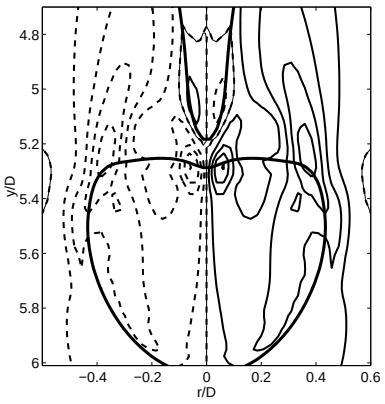

Figure 4.23: Simulation.